On-Chip Temporal Telescope via Moving Index Fronts

Mahmoud A. Gaafar, Abdellatif Bouchalkha, Chaouki Kasmi, and Felix Vega

***Abstract*—We propose a scheme for an on-chip signal pulse compression using a temporal telescope formed by a pump-induced moving refractive index front. To the best of our knowledge, this is the first numerical demonstration of such a concept using moving index perturbations. We numerically study the signal dynamics under the influence of a moving refractive index front in optical waveguides, revealing analogies to relativistic event horizon physics. Our simulations show that a free-carrier-induced refractive index front, which lowers the refractive index and induces a blue shift in the waveguide's band diagram, can overtake and trap a signal pulse, dynamically accelerating it to the front's velocity. As the interaction continues, the signal is eventually released from the front and transitions into a new velocity regime. This process of trapping, acceleration, and release mirrors the behavior of light near gravitational horizons, with the release phase analogous to light escaping a white hole. These results pave the way for new approaches in nonlinear optics and signal processing using compact, chip-scale systems.**

***Index Terms*—Non-linear signal manipulation, on-chip dynamic pulse compression, optical analogue of event horizon.**

I. Introduction

THE capability of manipulating and characterizing ultrafast optical signals is at the heart of modern technologies, including high-speed optical communications [1], [2], quantum information processing [3], biomedical imaging [4] and ultrafast spectroscopy [5]. In parallel, progress in nonlinear photonic platforms has enabled powerful techniques of all-optical signal processing [6], [7], [8], [9], making it possible to generate, reshape, and measure complex optical waveforms on timescales far beyond the conventional electronic systems.

A key technique in this domain is the temporal telescope based on the time-lens principle, which enables the temporal equivalent of spatial beam shaping [8], [10]. Such architectures allow for temporal magnification or compression of optical signals and have been demonstrated using four-wave mixing [11] or electro-optic modulation [12]. These systems often require specially prepared pump sources and intricate control of dispersion, which limits the integration.

Received 6 October 2025; revised 7 January 2026; accepted 9 January 2026. Date of publication 15 January 2026; date of current version 26 January 2026. *(Corresponding author: Mahmoud A. Gaafar.)*

Mahmoud A. Gaafar is with Technology Innovation Institute (TII), Abu Dhabi SE45-01, UAE, also with the Department of Physics, Faculty of Science, Menoufia University, Menoufia 6131567, Egypt, and also with the Institute of Optical, Electronic Materials, Hamburg University of Technology TUHH, 21073 Hamburg, Germany (e-mail: mahmoud.gaafar@tii.ae).

Abdellatif Bouchalkha, Chaouki Kasmi, and Felix Vega are with Technology Innovation Institute (TII), Abu Dhabi SE45-01, UAE.

Digital Object Identifier 10.1109/JPHOT.2026.3654559

An alternative paradigm leverages dynamic refractive index perturbations to reshape optical waveforms [13], [14], [15], [16], [17], [18], [19], [20], [21], [22], [23], [24]. Such fronts can be induced within the same waveguide via either the process of two-photon absorption (TPA)-generated free carriers [13], [16], [25] or through the Kerr effect [26], [27]. As these fronts propagate, they create localized changes in group velocity and dispersion, enabling a new class of compact, on-chip methods for real-time temporal control.

Recent work in time-varying photonics has opened new topics by treating time as an active design parameter [21], [22]. This concept has led to novel phenomena such as time mirrors, frequency shifts without moving parts, as well as nonreciprocal signal propagation. Temporal boundaries allow for new ways to control energy flow, signal direction, and bandwidth, often bypassing traditional limitations such as time-reversal symmetry [22]. These developments open doors for optical systems that operate not just in space but also dynamically in time. Building on this idea, our work shows how a moving refractive index front can act like a temporal lens, compressing signals in time much like a regular lens focuses light in space. This brings the advantages of time-domain control to chip-scale platforms, with potential for scalable and high-speed signal processing.

A recent study by Babushkin et al. adds further perspective by exploring a "time cavity" i.e. a moving refractive index discontinuity created by a soliton, which traps weak probe waves [28]. Unlike traditional cavities, this dynamic trap supports bound states even with shallow potential depth. While their system relies on soliton-induced index changes and ours uses free-carrier fronts, both approaches show the power of time-domain refractive index control for light.

In our work, we present a chip-integrated temporal telescope that compresses optical pulses by letting them interact with a moving index front. The signal is first caught and accelerated—similar to the first $2f$ stage in spatial imaging—and then released into a different dispersion regime, completing the compression in the second $2f$ stage. This method avoids complex modulation or synchronization schemes, making it an appealing solution for compact and scalable integrated photonics.

II. Results

Building on the concept introduced above, we now describe the implementation of the proposed temporal telescope based on a moving free-carrier-induced refractive index front.

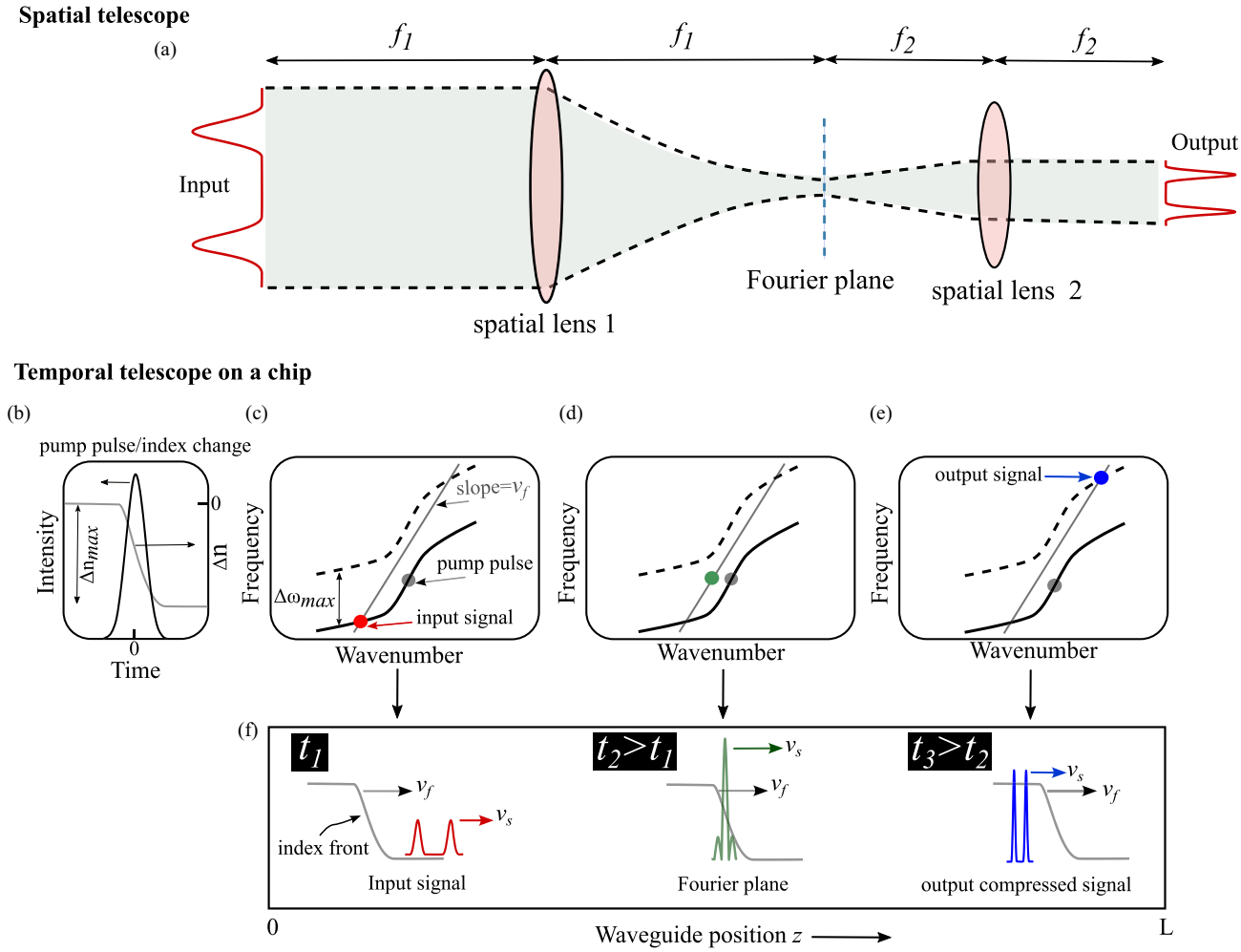

Fig. 1. (a) Schematic of a simplified conventional spatial 4-f imaging system. (b)–(f) Conceptual illustration of the proposed chip-integrated, free-carrier-induced temporal telescope. (b) A pump pulse generates a free-carrier-induced moving refractive index front. (c)–(e) Evolution of the signal pulse within the waveguide, shown alongside the band diagram. The solid curve represents the original dispersion relation, while the dashed curve shows the modified band diagram in the presence of free carriers. The gray line indicates the phase continuity line. The red, green, and blue dots mark the spectral positions of the input, trapped, and output signals, respectively, while the gray circle denotes the frequency of the pump pulse that generates the index front. (f) Illustration of the temporal telescope action, showing the spatial profile of the signal pulse at three distinct time snapshots during its interaction with the moving index front (gray curve).

In practice, this front considered here originates from a strong, co-propagating pump pulse that generates free carriers via TPA process. The resulting free-carrier induces a transient refractive-index change $\Delta n_{\mathrm{FC}}(t, z)$ which propagates at the pump group velocity. Within the time-dependent linear Schrödinger equation [29], this perturbation represented through the term $iq(t, z)$, where $q(t, z)$ represents the spatiotemporal profile of the free-carrier-induced index front.

Fig. 1(b)–(f) illustrates the operating principle of the proposed system as a temporal $4f$ imaging configuration, analogous to a conventional spatial telescope shown in Fig. 1(a). In this scheme, a slow-light signal pulse, initially located on the left branch of the waveguide band diagram (red filled circle in Fig. 1(c)), is overtaken by a fast-propagating free-carrier-induced index front (grey filled circle). As a result of this interaction, the signal is captured by the moving front, accelerated, and shifted to a higher optical frequency, corresponding to a faster propagation mode (green filled circle in Fig. 1(d)). With further interaction, the signal is released from the front and transferred into a different dispersion regime (blue filled circle in Fig. 1(e)). The gray line denotes the *phase continuity line* [16], [30], whose slope matches the velocity of the pump pulse.

It is important to highlight that the band diagram can be divided into three distinct branches, each characterized by a different slope, which corresponds to a specific group velocity:

- The *left branch* exhibits the lowest slope, indicating the smallest group velocity.
- The *middle branch* has the steepest slope, corresponding to the highest group velocity and the strongest group velocity dispersion.
- The *right branch* presents a slope greater than the left but smaller than the middle, implying an intermediate group velocity.

In this configuration, a slow-light, double-peaked signal pulse, initially located on the left branch of the dispersion relation, becomes trapped by a fast co-propagating front (grey dot). As the signal interacts with the moving index front, it undergoes a blue shift and is accelerated to match the front's velocity. This

dynamic trapping process effectively transforms the input signal into its temporal Fourier transform, represented by the green dot in Fig. 1(d) [13]. The trapping of the signal pulse by the moving refractive-index front corresponds to the *optical push-broom* effect in waveguides with hyperbolic dispersion [26], [31]. In this regime, a slow-light signal is accelerated to the front velocity without undergoing transmission or reflection, remaining confined within the moving front and experiencing temporal compression as the optical energy is concentrated in the front region.

As the interaction continues within the waveguide, the signal remains trapped and is further blue-shifted along the phase continuity line, eventually reaching the right branch of the dispersion relation—now in the switched (free-carriers-modified) state, marked by the blue dot in Fig. 1(e). At this stage, the signal pulse propagates with a velocity lower than that of the front, indicating that it has been released behind the front.

Since the dispersion of the right (final) branch is higher than that of the left (initial) branch, the signal pulse undergoes temporal compression analogous to spatial compression in a conventional telescope (Fig. 1(a)). This engineered dispersion profile is key to realizing the proposed temporal telescope and marks a significant advancement over earlier study [31], which focused on Fourier transform operations using hyperbolic dispersion relations. In that previous approach, the output signal represented only the Fourier-transformed version of the input, with limited preservation of its original temporal or spatial features. In contrast, the present work leverages a carefully designed dispersion landscape that not only enables Fourier transformation, but also allows for full temporal reconstruction and compression of the input signal. As a result, the waveform is recovered in a compressed form. Fig. 1(f) presents a schematic view of the interaction between the index front and the signal pulse at three distinct temporal stages: the input, its Fourier transform, and the compressed output.

The scenario illustrated in Fig. 1(b)–(f) not only demonstrates the functionality of a temporal telescope but also reveals a rich dynamical process involving the trapping, acceleration, and release of an optical signal. As a fast-moving refractive index front—lowering the local refractive index—overtakes a slow-light signal pulse, the pulse becomes confined within the front and accelerates to match its velocity. This interaction results in a frequency upshift and a transition into a new dispersion regime upon release.

This behavior is closely related to effects known from gravitational event-horizon physics [32]. Similar to light trapping near a black hole, the signal is confined and temporally compressed when interacting with a refractive-index front moving faster than its group velocity. Its subsequent release from the front resembles light escaping from a white-hole horizon.

To demonstrate the operation of the front-induced temporal telescope and elucidate the stages of pulse compression, we numerically solve the time-dependent linear Schrödinger equation using the split-step Fourier method [29]. The evolution of the slowly varying envelope of the signal, denoted by $a(t, z)$, is governed by:

$$\frac{\partial a}{\partial t} = v_d \frac{\partial a}{\partial z} + \sum_{m=2}^{\infty} i^{m+1} \frac{\omega_m}{m!} \frac{\partial^m a}{\partial z^m} + iq(t, z) \tag{1}$$

Here, $z = Z - v_f t$ represents the longitudinal coordinate in a reference frame moving with the front, while t denotes the time. Z corresponds to the longitudinal position in the laboratory frame. The coefficients $\omega_m = \frac{d^m \omega}{d\beta^m}\big|_{\beta_0}$ arise from the Taylor series expansion of the dispersion relation $\omega(\beta)$ evaluated at the propagation constant β_0, which is associated with the pump frequency. The term $q(t, z)$ describes a spatially localized modification of the dispersion, introduced by the nonlinearity induced through the pump [29].

We simulate the interaction between a linearly propagating index front and a double-peaked input signal pulse, as shown in Fig. 2(a). The input pulse is unchirped, with a temporal width of 29 ps. The refractive-index front has a temporal duration of 6.6 ps, corresponding to a spatial width of 1 mm, and propagates at a velocity of $0.5c$, where c denotes the speed of light. The dispersion relation employed in the simulation is modeled as piecewise linear and is shown in the moving frame (retarded frame) in Fig. 2(b).

The front is assumed to originate from free-carrier-induced refractive index modulation, which lowers the refractive index and results in a blue shift of the band diagram. The strength of the front is characterized through the induced refractive-index change, expressed in the band diagram as a maximum vertical frequency shift of 1 THz, as indicated by the dashed black curve in Fig. 2(b).

In the present model, free-carrier recombination is neglected, as carrier lifetimes in typical semiconductor waveguides (several hundreds of picoseconds to nanoseconds) [33] are much longer than both the pump duration and the signal interaction time. While free-carrier absorption and additional losses associated with TPA-induced carrier generation are inherently present, their impact might be minimized by operating at moderate carrier densities and over short interaction lengths, such that the refractive-index step dominates the signal dynamics. A key requirement is that the front exhibits a sufficiently sharp rise time compared to the temporal features of the signal, ensuring that it acts as a well-defined moving boundary.

The red circle marks the spectral location of the input signal, while the gray circle denotes the frequency of the pulse generating the index front. Based on their positions on the dispersion relation, the group velocities of the input signal (left branch), the front (middle branch), and the output signal (right branch) are $0.25c$, $0.5c$, and $0.475c$, respectively.

The temporal evolution of the signal in the co-moving frame is illustrated in Fig. 2(c). The pseudo-color map represents the pulse power, and the dashed orange lines indicate the boundaries of the moving index front. As shown, the signal becomes trapped and accelerated until it reaches the front's velocity. Continued interaction leads to deceleration and release of the signal, accompanied by both temporal and spatial compression.

Fig. 3(a)–(c) illustrates the characteristics of the signal pulse in the spatial domain, While the corresponding spatial frequency

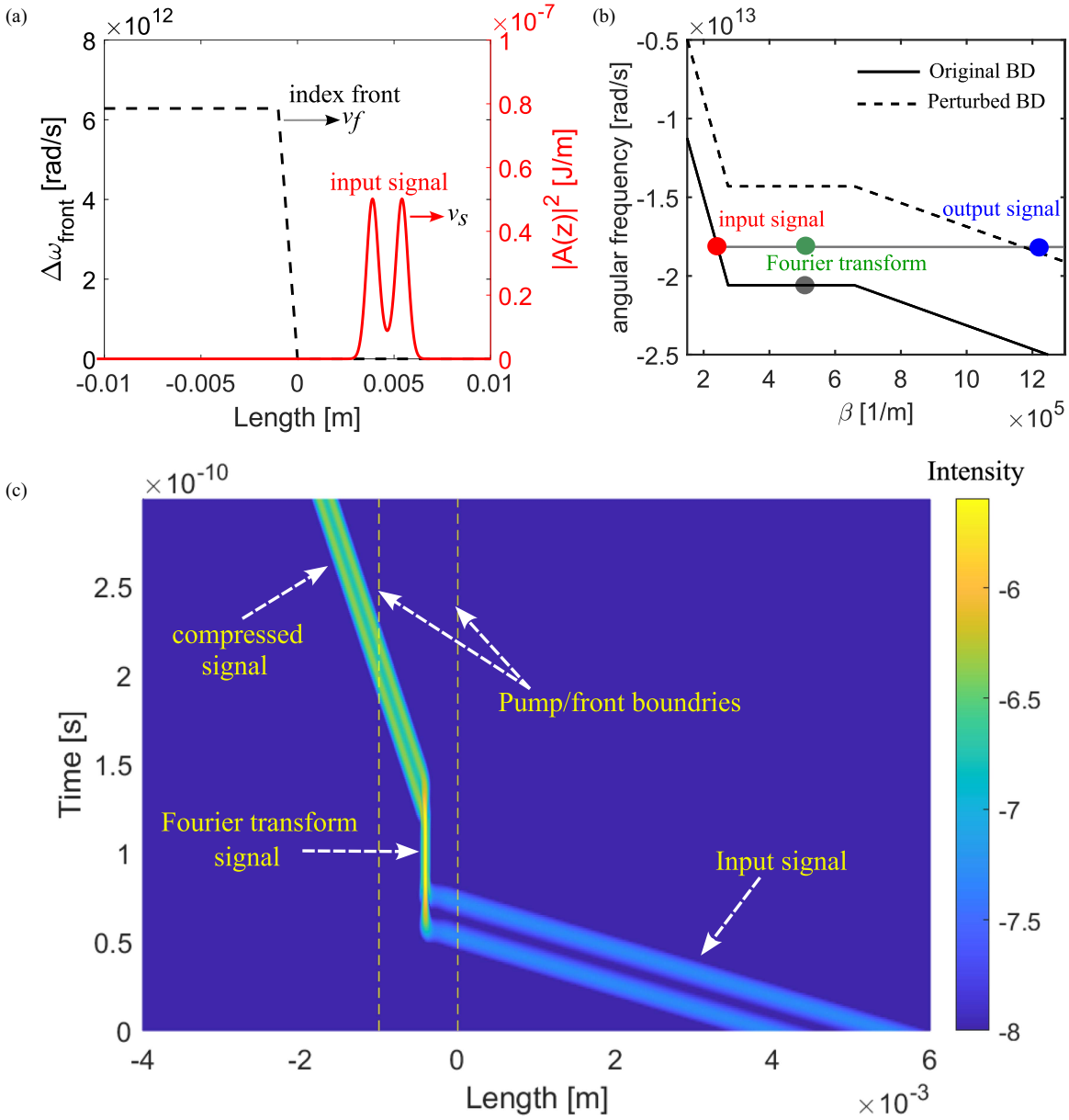

Fig. 2. (a) Relative position of the signal (red curve) within the moving free-carrier-induced refractive index front (dashed curve) at the input ($t = 0$). (b) Band diagram shown in the reference frame co-moving with the front (i.e., the retarded frame of the simulated system). The solid curve represents the original dispersion relation, while the dashed curve corresponds to the maximally perturbed band diagram due to free-carrier generation. The red, green and red circles indicate the spectral position of the input, trapped, and output signals, respectively, while the gray circle denotes the frequency of the pump pulse that generates the index front. (c) Temporal evolution of the double-peaked signal pulse in the moving frame. The input pulse duration is 29 ps, the waveguide length is $L = 4.4$ cm, and the maximum frequency shift in the band diagram is $\Delta\omega_{\max} = 1$ THz, induced by the pump. Orange dashed lines represent the spatial/temporal boundaries of the index front.

domain is illustrated in Fig. 3(d)–(f). The plots represent three stages of the signal evolution: the input signal (before interaction with the index front), the trapped signal (during interaction), and the output signal (after being released from the front).

Several key observations can be concluded from this figure. First, the spatial frequency of the input signal is transformed into spatial information as the signal becomes trapped and accelerated by the moving index front (Fig. 3(b) and (e)). Second, after the signal is released from the front, its spatial frequency bandwidth increases by approximately a factor of 10, resulting in a corresponding temporal compression of the pulse by approximately the same factor (Fig. 3(c) and (f)). This clearly confirms the operation of the system as a temporal telescope.

It is important to note that the compression factor depends on the relative slopes, and consequently the group velocity dispersions of the initial and final branches of the dispersion relation, denoted as D_1 and D_2, respectively. An increase in D_2 relative to D_1 leads to stronger compression.

We further investigate the ability of the temporal telescope to compress an arbitrary waveform or a highly structured input signal with multiple peaks (inset of Fig. 4). The signal's temporal evolution in the co-moving frame is shown in Fig. 4.

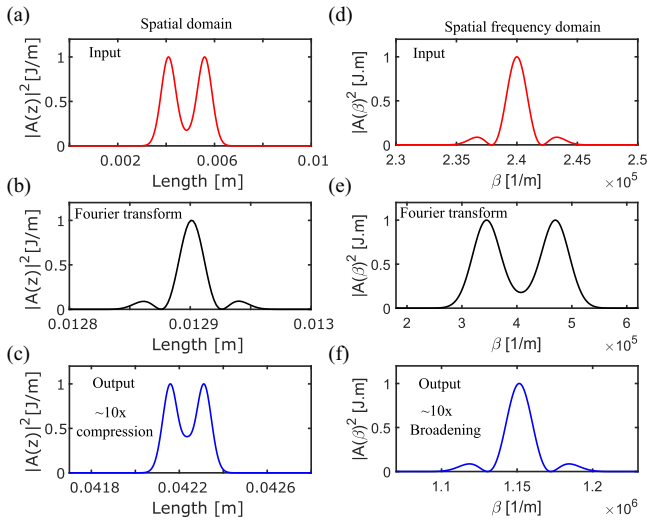

Fig. 3. (a)–(c) Spatial profiles of the signal pulse at three distinct stages within the waveguide: (a) input, (b) intermediate Fourier-transformed state, and (c) compressed output. (d)–(f) Corresponding spectral representations for each stage, respectively.

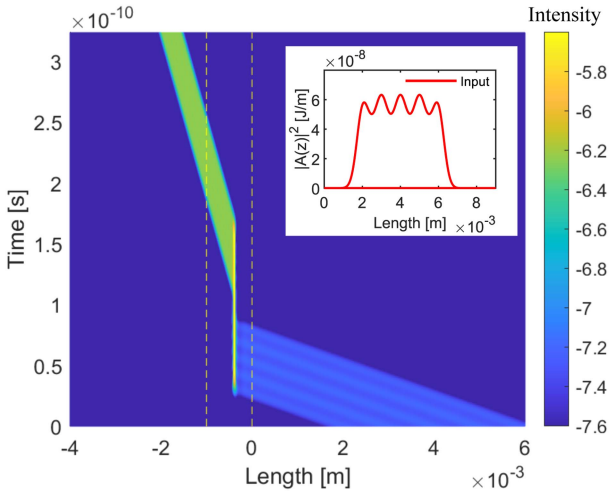

Fig. 4. Temporal evolution of the multi-peaked signal pulse (inset) in the reference frame co-moving with the front.

As illustrated, the multi-peaked input signal becomes trapped and accelerated until its velocity matches that of the moving index front. Continued interaction results in deceleration and release of the signal, accompanied by both temporal and spatial compression.

III. Conclusion

In summary, we have introduced an on-chip temporal telescope enabled by a pump-induced moving refractive index front, offering a new approach for signal pulse compression in integrated photonics. Through numerical analysis, we demonstrated how such a front can trap, accelerate, and release a signal pulse, leading to controlled temporal compression. The dynamics observed closely mirror the behavior of light near gravitational event horizons, providing a compelling optical analogue to curved spacetime phenomena. It is worth noting that free-carrier generation can introduce additional loss through free-carrier absorption; however, this might be mitigated by operating at moderate carrier densities and over short interaction lengths, such that the refractive-index step dominates the dynamics. Furthermore, the realization of this effect relies on a specifically engineered dispersion relation that supports the trapping mechanism. These results pave the way for potential applications in signal processing, nonlinear optics, and analogue gravity experiments [32], [34].

Declaration of Competing Interest

The authors declare no competing financial or personal interests.

Data Availability

Data available on reasonable request from the corresponding author.

References

[1] K. G. Petrillo and M. A. Foster, "Full 160-gb/s OTDM to 16x10-gb/s WDM conversion with a single nonlinear interaction," *Opt Exp.*, vol. 21, no. 1, pp. 508–518, Jan. 2013.

[2] N. K. Fontaine, R. P. Scott, and S. Yoo, "Dynamic optical arbitrary waveform generation and detection in InP photonic integrated circuits for Tb/s optical communications," *Opt. Commun.*, vol. 284, no. 15, pp. 3693–3705, 2011. [Online]. Available: https://www.sciencedirect.com/science/article/pii/S0030401811003166

[3] A. B. U'Ren, E. Mukamel, K. Banaszek, and I. A. Walmsley, "Managing photons for quantum information processing," *Philos. Trans.: Math. Phys. Eng. Sci.*, vol. 361, no. 1808, pp. 1493–1506, 2003. [Online]. Available: http://www.jstor.org/stable/3559255

[4] K. E. Sheetz and J. Squier, "Ultrafast optics: Imaging and manipulating biological systems," *J. Appl. Phys.*, vol. 105, no. 5, Mar. 2009, Art. no. 051101, doi: 10.1063/1.3081635.

[5] Y. Okawachi, R. Salem, M. A. Foster, A. C. Turner-Foster, M. Lipson, and A. L. Gaeta, "High-resolution spectroscopy using a frequency magnifier," *Opt. Exp.*, vol. 17, no. 7, pp. 5691–5697, Mar. 2009. [Online]. Available: https://opg.optica.org/oe/abstract.cfm?URI=oe-17-7-5691

[6] M. A. Foster, R. Salem, D. F. Geraghty, A. C. Turner-Foster, M. Lipson, and A. L. Gaeta, "Silicon-chip-based ultrafast optical oscilloscope," *Nature*, vol. 456, no. 7218, pp. 81–84, Nov. 2008, doi: 10.1038/nature07430.

[7] T. Hirooka and M. Nakazawa, "All-optical 40 GHz time-domain fourier transformation using XPM with a dark parabolic pulse," presented at the Optical Fiber Communication Conference, San Diego, CA, USA, Feb. 24–28, 2008, Paper OThG5. [Online]. Available: https://opg.optica.org/abstract.cfm?URI=OFC-2008-OThG5

[8] R. Salem, M. A. Foster, A. C. Turner, D. F. Geraghty, M. Lipson, and A. L. Gaeta, "Optical time lens based on four-wave mixing on a silicon chip," *Opt. Lett.*, vol. 33, no. 10, pp. 1047–1049, May 2008. [Online]. Available: https://opg.optica.org/ol/abstract.cfm?URI=ol-33-10-1047

[9] R. Salem, M. A. Foster, A. C. Turner-Foster, D. F. Geraghty, M. Lipson, and A. L. Gaeta, "High-speed optical sampling using a silicon-chip temporal magnifier," *Opt. Exp.*, vol. 17, no. 6, pp. 4324–4329, Mar. 2009. [Online]. Available: https://opg.optica.org/oe/abstract.cfm?URI=oe-17-6-4324

[10] R. Salem, M. Foster, and A. Gaeta, "Application of space–time duality to ultrahigh-speed optical signal processing," *Adv. Opt. Photon.*, vol. 5, Aug. 2013, Art. no. 274.

[11] M. A. Foster, R. Salem, Y. Okawachi, A. C. Turner-Foster, M. Lipson, and A. L. Gaeta, "Ultrafast waveform compression using a time-domain telescope," *Nature Photon.*, vol. 3, no. 10, pp. 581–585, Oct. 2009, doi: 10.1038/nphoton.2009.169.

[12] M. Karpiński, M. Jachura, L. J. Wright, and B. J. Smith, "Bandwidth manipulation of quantum light by an electro-optic time lens," *Nature Photon.*, vol. 11, no. 1, pp. 53–57, Jan. 2017, doi: 10.1038/nphoton.2016.228.

[13] M. Gaafar, T. Baba, M. Eich, and A. Petrov, "Front-induced transitions," *Nature Photon.*, vol. 13, pp. 737–748, Sep. 2019.

[14] H. Li, Y. Gao, D. Fan, and L. Zhang, "Dispersive wave manipulation by the spectral heaviside step phase modulation," *Opt. Lett.*, vol. 48, no. 24, pp. 6529–6532, Dec. 2023. [Online]. Available: https://opg.optica.org/ol/abstract.cfm?URI=ol-48-24-6529

[15] B. W. Plansinis, W. R. Donaldson, and G. P. Agrawal, "What is the temporal analog of reflection and refraction of optical beams?," *Phys. Rev. Lett.*, vol. 115, Oct. 2015, Art. no. 183901, doi: 10.1103/PhysRevLett.115.183901.

[16] M. A. Gaafar et al., "Reflection from a free carrier front via an intraband indirect photonic transition," *Nature Commun.*, vol. 9, no. 1, Apr. 2018, Art. no. 1447, doi: 10.1038/s41467-018-03862-0.

[17] K. Kondo and T. Baba, "Slow-light-induced doppler shift in photonic-crystal waveguides," *Phys. Rev. A*, vol. 93, Jan. 2016, Art. no. 011802, doi: 10.1103/PhysRevA.93.011802.

[18] L. Zhang, Q. Huang, W. Cai, C. Xu, Y. Gao, and D. Fan, "Distance controlled resonant radiation from modulated airy pulses," *Results Phys.*, vol. 52, 2023, Art. no. 106814. [Online]. Available: https://www.sciencedirect.com/science/article/pii/S2211379723006071

[19] H. Li, X. Zhang, J. Zhang, D. Pierangeli, L. Zhang, and D. Fan, "Boosting dispersive wave emission via spectral phase shaping in nonlinear optical fibers," *Results Phys.*, vol. 19, 2020, Art. no. 103518. [Online]. Available: https://www.sciencedirect.com/science/article/pii/S2211379720319690

[20] R. Dekker, A. Driessen, T. Wahlbrink, C. Moormann, J. Niehusmann, and M. Först, "Ultrafast kerr-induced all-optical wavelength conversion in silicon waveguides using 1.55 μm femtosecond pulses," *Opt. Exp.*, vol. 14, no. 18, pp. 8336–8346, Sep. 2006. [Online]. Available: https://opg.optica.org/oe/abstract.cfm?URI=oe-14-18-8336

[21] J. B. Pendry, E. Galiffi, and P. A. Huidobro, "Gain in time-dependent media–A new mechanism," *J. Opt. Soc. America B*, vol. 38, no. 11, pp. 3360–3366, 2021, doi: 10.1364/JOSAB.427682.

[22] E. Galiffi et al., "Photonics of time-varying media," *Adv. Photon.*, vol. 4, no. 1, 2022, Art. no. 014002, doi: 10.1117/1.AP.4.1.014002.

[23] S. Bose et al., "Manipulation of single-photon wave packets via kerr-nonlinear refractive index fronts," in *Proc. Conf. Lasers Electro- Opt. Europe Eur. Quantum Electron. Conf.*, 2023, pp. 1–1.

[24] H. Li, Z. Wang, Z. Xie, D. Fan, and L. Zhang, "Manipulating dispersive wave emission via temporal sinusoidal phase modulation," *Opt. Exp.*, vol. 31, no. 4, pp. 6296–6303, 2023, doi: 10.1364/OE.477198.

[25] M. A. Gaafar, J. Holtorf, M. Eich, and A. Petrov, "Pulse time reversal and stopping by a refractive index front," *APL Photon.*, vol. 5, no. 8, 2020, Art. no. 080801, doi: 10.1063/5.0007986.

[26] N. G. R. Broderick, D. Taverner, D. J. Richardson, M. Ibsen, and R. I. Laming, "Optical pulse compression in fiber bragg gratings," *Phys. Rev. Lett.*, vol. 79, pp. 4566–4569, Dec. 1997, doi: 10.1103/PhysRevLett.79.4566.

[27] A. Billat, S. Cordette, Y.-P. Tseng, S. Kharitonov, and C.-S. Brès, "High-power parametric conversion from near-infrared to short-wave infrared," *Opt. Exp.*, vol. 22, no. 12, pp. 14341–14347, Jun. 2014. [Online]. Available: https://opg.optica.org/oe/abstract.cfm?URI=oe-22-12-14341

[28] I. Babushkin, O. Melchert, U. Morgner, and A. Demircan, "Photon trapping in a time cavity flying with the speed of light," in *Preprint on Research Square*, 2022. Accessed: Sep. 2022. [Online]. Available: https://assets-eu.researchsquare.com/files/rs-1982423/v1_covered.pdf?c=1662734730

[29] M. A. Gaafar, H. Renner, A. Y. Petrov, and M. Eich, "Linear schrödinger equation with temporal evolution for front induced transitions," *Opt. Exp.*, vol. 27, no. 15, pp. 21273–21284, Jul. 2019. [Online]. Available: https://opg.optica.org/oe/abstract.cfm?URI=oe-27-15-21273

[30] M. A. Gaafar, A. Y. Petrov, and M. Eich, "Free carrier front induced indirect photonic transitions: A new paradigm for frequency manipulation on chip," *ACS Photon.*, vol. 4, no. 11, pp. 2751–2758, Nov. 2017, doi: 10.1021/acsphotonics.7b00750.

[31] M. A. Gaafar, H. Renner, M. Eich, and A. Y. Petrov, "Fourier optics with linearly tapered waveguides: Light trapping and focusing," *APL Photon.*, vol. 6, no. 6, Jun. 2021, Art. no. 066108, doi: 10.1063/5.0050770.

[32] T. G. Philbin, C. Kuklewicz, S. Robertson, S. Hill, F. König, and U. Leonhardt, "Fiber-optical analog of the event horizon," *Science*, vol. 319, no. 5868, pp. 1367–1370, 2008. [Online]. Available: https://www.science.org/doi/abs/10.1126/science.1153625

[33] R. A. Soref and B. R. Bennett, "Electrooptical effects in silicon," *IEEE J. Quantum Electron.*, vol. 61, no. 3, 2025, Art. no. 0600507. [Online]. Available: https://api.semanticscholar.org/CorpusID:123616317

[34] S. A. Cummer, J. Christensen, and A. Alù, "Analogue transformations in physics and their application to acoustics," *Sci. Rep.*, vol. 3, 2013, Art. no. 2607. [Online]. Available: https://www.nature.com/articles/srep02607